Molecular Dynamics Simulations of Classical Stopping Power

Paul E. Grabowski,[1] Michael P. Surh,[2] David F. Richards,[2] Frank R. Graziani,[2] and Michael S. Murillo[1,*]

[1]*Computational Physics and Methods Group, Los Alamos National Laboratory, Los Alamos, New Mexico 87545, USA*

[2]*Lawrence Livermore National Laboratory, Livermore, California 94550, USA*

(Received 20 August 2013; published 19 November 2013)

Molecular dynamics can provide very accurate tests of classical kinetic theory; for example, unambiguous comparisons can be made for classical particles interacting via a repulsive $1/r$ potential. The plasma stopping power problem, of great interest in its own right, provides an especially stringent test of a velocity-dependent transport property. We have performed large-scale ($\sim 10^4$–10^6 particles) molecular dynamics simulations of charged-particle stopping in a classical electron gas that span the weak to moderately strong intratarget coupling regimes. Projectile-target coupling is varied with projectile charge and velocity. Comparisons are made with disparate kinetic theories (both Boltzmann and Lenard-Balescu classes) and fully convergent theories to establish regimes of validity. We extend these various stopping models to improve agreement with the MD data and provide a useful fit to our results.

DOI: 10.1103/PhysRevLett.111.215002 PACS numbers: 52.27.Gr, 05.20.Dd, 52.25.Dg, 52.65.Yy

The nonequilibrium statistical mechanics of particles interacting via long-range forces is an outstanding challenge. Many-body simulations can provide insight into the wide range of complex behaviors that result [1–4]. Simulations are particularly valuable for model validation when precise data are lacking in high energy-density physics experiments [5,6]. Whereas most transport phenomena represent averages over thermal velocities, charged particle stopping depends on a single projectile velocity. Thus stopping power provides a velocity-resolved probe of the underlying collision integrands and offers greater insight into the accuracy of energy and particle flow models, including temperature relaxation [7–9], diffusion [10,11], and electrical and thermal conductivity [12,13]. Improved knowledge of stopping power in high energy-density physics environments also directly impacts ion-based fast ignition [14], alpha particle deposition in thermonuclear fuels [15], and heavy ion fusion [16].

Because molecular dynamics (MD) cannot include quantum scattering and recombination exactly, we consider a purely classical repulsive Coulomb system of a negatively charged point projectile interacting with a one component electron gas target. Theoretical models can be formulated identically, so the MD provides a rigorous test of stopping power models [17]; insights can then be extrapolated to real matter. Within this system we vary both the intratarget and projectile-target coupling over large ranges to provide the greatest insight into the models. We vary the target temperature at fixed density to span weak to moderately strong intratarget coupling, and we vary projectile charge and velocity to influence projectile-target coupling.

In this Letter, we compare theoretical models of charged-particle stopping [17–24] with numerically exact, classical, nonrelativistic MD simulations. The underlying kinetic theories were chosen from the Lenard-Balescu (LB) class (weak scattering in a dense environment), the Boltzmann (B) class (strong scattering in a dilute environment), and convergent kinetic theories (CKT) [25]. We delimit regions of validity for these various models and quantify the importance of strongly coupled nonlinear binary collisions and collective phenomena. We develop nonlinear screening models (beyond Debye-Hückel) to better describe these effects and obtain accurate expressions for classical stopping. We introduce a new formula for classical charged particle stopping which is more accurate over a larger parameter space compared to commonly used expressions.

Our simulations use the massively parallel MD code, ddcMD [26,27], to treat long range forces. We varied the target temperature at fixed density $n_e = 1.03 \times 10^{20}$ cm^{-3} to obtain three values for the intratarget coupling parameter $\Gamma = q_e^2/(r_0 T) = 0.1, 1, 10$. Here, q_e is the target charge, T is the target temperature in energy units, and $r_0 = (4\pi n_e/3)^{-1/3}$ is the Wigner-Seitz radius. Projectile-target coupling was varied by selecting three projectile charges $Z = -1, -2, -10$ with projectile and target-particle masses consistent with the magnitude of the charge: $m = m_{\mathrm{H}}, m_{\mathrm{He}}, m_{\mathrm{Ne}}, m_e$. Together these conditions define a matrix of nine physical conditions. For each of the nine cases, projectile velocities were selected in the range $v/v_{\mathrm{th}} \sim 0.1$–$40$, where $v_{\mathrm{th}} = \sqrt{T/m_e}$ is the thermal velocity of the target particles.

Converged stopping behavior for the fastest projectiles considered required a numerical time step of 10^{-5} to 10^{-4} fs. Long simulations were performed, typically 100 fs to relax transients followed by 300 fs (172 ω_p^{-1}) of data collection. For fast projectiles, a weak Langevin thermostat (decay time 30–100 fs) was used to suppress target heating by the projectile; this did not affect the stopping. Fast charged particles generate wake potentials of large spatial extent, problematic for a finite simulation domain with

periodic boundary conditions. Prior work [28,29] corrected for the missing long-wavelength contributions using a model. To avoid such a model dependence we employed large cubic cells (10–100 Debye lengths on an edge, or roughly 64 K − 1 M particles) and chose the initial projectile velocity to be a permutation of $\hat{v} = (1, \sqrt{\phi}, \phi)$, with $\phi = (1 + \sqrt{5})/2$, the golden ratio, minimizing overlap or interaction with periodic projectile wakes. Our MD results are shown in the Figs. 1, 2, 4, and 5. Multiple independent replicas establish error bars; nearly 900 simulations are included. We plot the stopping power, $-d\tilde{E}/dx$, versus velocity $\tilde{v}$, where $d\tilde{E}/dx = (dE/dx)(1+g)^{2/3}/(Z^2 q_e^2/\lambda_D^2)$, $\tilde{v} = v/[v_{\rm th}(1+g)^{1/3}]$, $g = \sqrt{3}|Z|\Gamma^{3/2}$, and $\lambda_D = r_0/\sqrt{3\Gamma}$ is the Debye-Hückel (DH) screening length.

We find that the stopping rates determined by our MD simulations are accurately described by the expression

$$\frac{d\tilde{E}}{dx} \approx -R(w)\left[G(w)\ln\left(e^{1/2} + \frac{\alpha + w^2}{g_0}\right) + H(w)\right], \qquad (1)$$

where

$$R(w) = \frac{[M_1 + bM_2(w)w^2](1+g)^{2/3}}{w^2(1+bw^2)},$$
$$M_1 = s\frac{\ln(1+\alpha e^{-1/2}/[g(1+aZ^2 g)])}{\ln(1+\alpha e^{-1/2}/g_0)},$$
$$M_2(w) = \frac{1}{s^2}\frac{\ln(1+s^3w^3/g)}{\ln(1+w^3/g_0)}, \qquad (2)$$
$$G(w) = \mathrm{erf}\left(\frac{w}{\sqrt{2}}\right) - \sqrt{\frac{2}{\pi}}we^{-w^2/2},$$
$$H(w) = \frac{w^4 \ln w}{12 + w^4} - \frac{w^3}{3\sqrt{2\pi}}e^{-w^2/2}.$$

Here, $\alpha = 4\exp(-2\gamma)$, γ is Euler's constant, 0.577216..., $s = d(1+cg)^{1/3}$, $w = v/(v_{\rm th}s)$, and the fit parameters are $a = 1.04102 \times 10^{-5}$, $b = 0.183260$, $c = 0.116053$, $d = 0.824982$, and $g_0 = 2.03301 \times 10^{-3}$. Equation (1) is Eq. (35) of Ref. [30] evaluated at $g = g_0$, with an altered Coulomb logarithm, the velocity rescaled by s, and the stopping power rescaled by M_1 and M_2 at low and high velocities, respectively. Its low velocity limit is $-(1+g)^{2/3}\ln\{1+\alpha e^{-1/2}/[g(1+agZ^2)]\}(v/v_{\rm th})\sqrt{2/9\pi}$, which matches the Brown-Preston-Singleton (BPS) model [19] at weak coupling and our MD simulations at strong coupling. The Bohr limit $[\ln(u^3/g)/u^2]$ [31] is preserved with the inclusion of M_2. The fit parameters, b, c, and d allow a good representation at moderate velocities. Equation (1) may be used to describe the light ionic component of heavy ion stopping power if the screening length is greater than the interparticle spacing, or the electron component if the classical distance of closest approach and the screening length are much greater than the thermal de Broglie wavelength. Over our nine simulation conditions, this fit has a maximum and root mean square error of 0.03 and 0.005, respectively, in units of $Z^2 q_e^2(1+g)^{-2/3}/\lambda_D^2$.

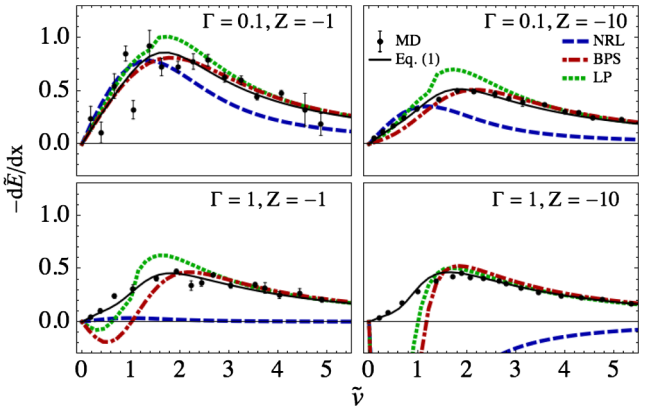

FIG. 1 (color online). Comparisons with three models (NRL, BPS, and LP) are made with the MD data for $\Gamma = 0.1$, 1, and two projectile charges $Z = -1$, -10. The fit of Eq. (1) is given by the thin black line.

Figure 1 compares Eq. (1) and our MD results to three models that are in wide use: the result from the NRL Plasma Formulary (NRL) [21], the BPS model [19], and the Li and Petrasso (LP) model [22]. We have evaluated the LP model with the u appearing in LP given by $\sqrt{v_{\rm th}^2 + v^2}$ and the NRL model using the Coulomb logarithm $\Lambda = 23 - \ln[|Z|(T/\mathrm{eV})^{-3/2}(n_e/\mathrm{cm}^{-3})^{1/2}]$. For $\Gamma = 0.1$ and $Z = -1$ the BPS model works well, the NRL model fails at high velocities, and the LP model suffers at the peak due to the use of a Heaviside theta function in its high-velocity correction. Other cases show larger deviations, particularly at low velocities when their Coulomb logarithms change sign. Only Eq. (1) matches the simulations for all conditions.

Figure 2 shows MD results for the four extreme limits of our nine cases; other cases give results between those shown. We compare the MD data with models of the LB class, which assume weak scattering with dynamical screening, thereby including many-body effects without invoking an *ad hoc* long-wavelength cutoff. This allows us to address three issues: the boundaries of a common LB-class model with respect to the three effective coupling parameters, the appropriate short-range cutoff, since the neglect of strong scattering in LB models leads to a divergence for classical systems, and the importance of dynamical screening. We will use these points for constructing improved models below. In Fig. 2 we plot

$$\frac{d\tilde{E}}{dx} = -\frac{2}{\pi\tilde{v}^2}\int_0^u d\tilde{\omega}\,\tilde{\omega}\int_0^Q dq q\frac{\mathrm{Im}[\epsilon(q,\tilde{\omega})]}{|\epsilon(q,\beta\tilde{\omega})|^2}, \qquad (3)$$

where $q = k\lambda_D$, $\tilde{\omega} = \omega/(kv_{\rm th})$, $u = v/v_{\rm th}$, and Q gives the short-range cutoff. We evaluate the dielectric response using the random-phase approximation (RPA) [30], setting β to zero or one selects static (SRPA) or dynamic (DRPA) screening, respectively. Traditionally, the cutoff Q is

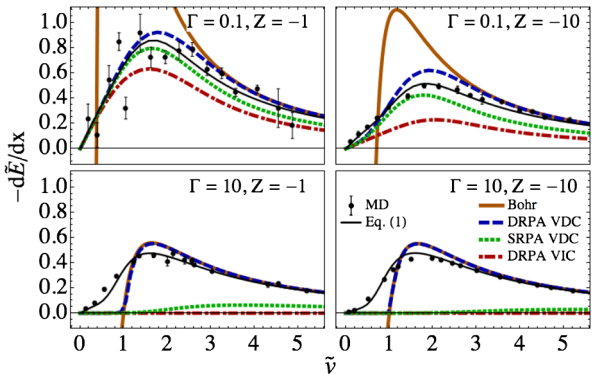

FIG. 2 (color online). Three LB-class stopping models, the Bohr model, and the MD data are shown for the four extreme cases in our data set. MD data (black points) are shown with five theory curves: the Bohr limit (solid orange), dynamic RPA velocity-dependent cutoff (dashed blue), dynamic RPA velocity-independent cutoff (dot-dashed red), and static RPA velocity-dependent cutoff (dotted green). The use of the velocity dependent cutoff with RPA is accurate everywhere except for small to moderate velocity. The fit of Eq. (1) is given by the thin black line.

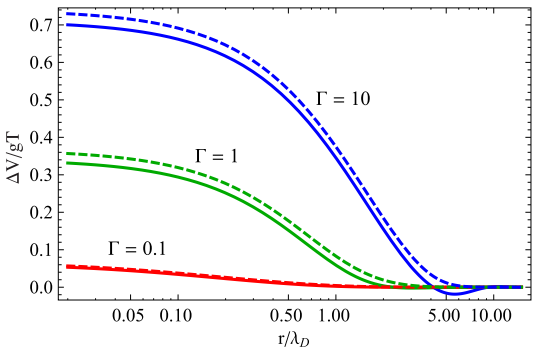

FIG. 3 (color online). Differences ΔV in nonlinear screening potentials from the linear mean field (DH), nonlinear mean field (PB, dashed), and beyond mean field (HNC, solid) are shown for three values of the Coulomb coupling constant.

chosen to correspond to the distance of closest approach, $Q_{\mathrm{VIC}} = \lambda_D T/Zq_e^2 = 1/g$, which we will refer to as the velocity independent cutoff (VIC). The VIC fails to produce the proper Bohr limit [31], $d\tilde{E}/dx = -\ln(u^3/g)/\tilde{v}^2$, so we also examine a velocity dependent cutoff (VDC) of the form $Q_{\mathrm{VDC}} = Q_{\mathrm{VIC}}(1+u^2)$ [28,29]. From Fig. 2 we see that dynamical screening and a VDC are *both* needed to reproduce the MD data at high velocity. While the static screening model ($\beta = 0$) is accurate at low velocities for the weakest coupling, $\Gamma = 0.1$, it is not generally useful. As with the models in Fig. 1, the model given in Eq. (3) tends to fail when either (projectile-target or intratarget) coupling parameter is large, with the most egregious errors at low velocity.

We now turn to the B class of models, which employ a binary cross section, and thereby include strong scattering. Because the bare Coulomb cross section has a long-wavelength divergence, we show T-matrix results that include many-body screening effects. This is typically included [28] with a projectile-target interaction of the DH form $V_{pt}(r) = Ze^2\exp(-r/\lambda_D)/r$. We compute the cross section numerically (see Ref. [32]). This DH-based T-matrix model is limited to weakly coupled plasmas for three reasons: T-matrix assumes an effective *binary* scattering, the colliding particles are uncorrelated, and DH screening is a linear, mean-field result. We remove the limitation of DH screening by computing the projectile-target interaction using the *nonlinear* Poisson-Boltzmann model and solving the hypernetted chain (HNC) equations [33] for the two-component plasma in the limit of one species (projectile) having vanishing concentration (see Ref. [34] for a similar usage of HNC). The nonlinear screening results are shown in Fig. 3, in which we see large deviations from DH for $\Gamma = 1, 10$. It is a limitation of the T-matrix formulation for strongly coupled plasmas that nonlinear screening potentials are not symmetric with respect to projectile and target. This leads to an ambiguity in the potential used in the cross section calculation. In the nonlinear case, a projectile-target binary interaction is different depending on whether the target particle or the projectile is considered to be screened by other nearby target particles. We chose the former because it isolates the projectile exchanging energy with the target. However, neither viewpoint is correct, and when the two predictions differ significantly neither is accurate. In all cases the screening models are static and the T-matrix method cannot accurately describe the projectile velocity dependence. We have shown this to be important in Fig. 2; thus, in Fig. 4 we only show low velocity results. In general we see that the T-matrix results yield a considerable improvement over those in Fig. 2 at low velocity at all coupling parameters, a regime important for alpha particle stopping [15].

In the limits of low velocity and large projectile-target mass ratio, Dufty and collaborators [35,36] have shown an exact relationship between the stopping power and the diffusion coefficient, D: $dE/dx = -vT/D$. Of course, this formula only shifts the difficulty to D, which can be obtained from MD via the velocity autocorrelation function (VACF). Hughto *et al.* [37] already did this calculation and provide a fit to their MD data ($\Gamma > 1$). We use their fit with the mass equal to our target particles [38,39]. Low velocity stopping is fundamentally described by a non-binary, nonlinear model, since the VACF contains the many-body physics of a particle entrained in a collective background. Our results are shown in Fig. 4, which are in excellent agreement with the MD data at low velocity at $\Gamma = 1$ and 10, despite the fact that the D used was for an equal mass system. Because weakly coupled data were not used to train the fit, the deviations at $\Gamma = 0.1$ are not surprising.

To improve upon the poor velocity dependence of the T-matrix models, we also compare with CKT models [25].

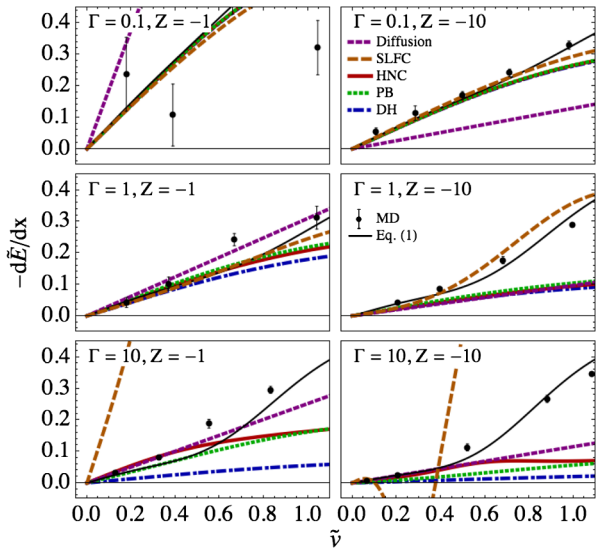

FIG. 4 (color online). T-matrix stopping power using three different screening potentials, Debye-Hückel (dot-dashed blue), Poisson-Boltzmann (dotted green), and HNC (solid red), shown with the diffusion model (short-dashed purple), SLFC (long-dashed orange), and MD data (points). The T-matrix model has the (known) defect of being inaccurate at high velocity, although the nonlinear screening potentials greatly improve the low velocity stopping power whenever the target-projectile coupling is large.

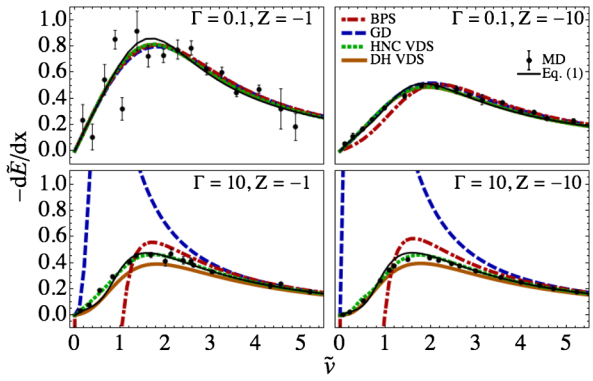

FIG. 5 (color online). A comparison of CKT models are shown, including BPS (dot-dashed red), GD (dashed blue), and improved T-matrix models that employ velocity-dependent screening lengths of two types [HNC (dotted green) and DH (solid orange)].

Because of its partial success (see Fig. 2), we modified the DRPA VDC model to include static local field corrections (SLFC) $G_{ij}(k)$ for the projectile-target mixture, including both a $1 - G_{tt}(k)$ in the target dielectric function and a projectile-target factor $1 - G_{pt}(k)$ in the numerator of the integrand in Eq. (3): this serves to make the LB model convergent while also including many-body physics in the short-wavelength cutoff. We see in Fig. 4 that this greatly improves the low velocity results. Dynamic LFCs would be needed for the model to apply at all velocities. The Gould-Dewitt (GD) model [40], which constructs a CKT by employing both LB and B type features, is compared with the previously presented CKT BPS model. A model developed previously [28,29,41] that employs a velocity-dependent DH screening length is also considered, and we extend that to our nonlinear potentials. Our velocity-dependent scaling procedure scales all lengths L in the potential as $L \to L\sqrt{1 + u^2(1 + \Gamma^3)^{1/4}}$, which empirically extends the prior work to strong coupling. The CKT comparisons are shown in Fig. 5 for the four corner cases of our data set. The models in this class agree very well at weak coupling. The GD model either offers no improvement over simpler models or does poorly. Comparison with the MD data reveals that the best model overall is our T-matrix model with velocity-dependent HNC screening.

In summary, we have produced accurate molecular dynamics results for charged particle stopping using simulations that cover a broad range of projectile-target couplings, intratarget couplings, and projectile velocities. These simulations employ orders of magnitude more particles than previous studies, allowing us to simulate long-wavelength wake structures. Our simulations utilized a purely classical plasma to allow for a model-independent comparison with theoretical models. We have provided a fit that accurately matches our MD results across the full range of temperature, velocity, and projectile charge we studied. We have compared our results with a very large range of differing theoretical models that originate from disparate branches of kinetic theory. Our data have allowed us to evaluate several stopping power models that are in wide use. We find that models in the LB class yield accurate results for high velocity and any coupling parameter, provided that a velocity-dependent cutoff and dynamical screening are used. However, low velocity stopping is poorly predicted by LB models for the more strongly coupled cases, which can be improved by the inclusion of LFCs. In the B class we compared our data with T-matrix models, including a new model that includes nonlinear screening. While these models yield good results for low velocity, they are quite inaccurate at even moderate velocities. We find that while the nonlinear screening is a marked improvement, there are ambiguities in its implementation because there is no unique nonlinear potential to be used in a binary cross section. To bridge the gap between LB and B class models we also considered CKT models. We find that the CKT models are in excellent agreement with each other for weak coupling. For strong intratarget coupling, the GD and BPS models fail, with the best model being our T-matrix model that employs HNC screening and a velocity-scaled screening length. Finally, we have compared our MD data with a stopping power model that relates stopping to diffusion and find very good agreement at low velocities, where that relationship should be accurate. Our MD results can readily distinguish among a very wide range of theoretical models.

The authors wish to thank Jim Glosli (LLNL) and A. Bruce Langdon (LLNL) for very useful conversations. This work is performed under the auspices of the U. S. Department of Energy by Lawrence Livermore National Laboratory under Contract DE-AC52-07NA27344, and parts have been authored by employees of the Los Alamos National Security, LLC. (LANS), operator of the Los Alamos National Laboratory under Contract No. DE-AC52-06NA25396 with the U.S. Department of Energy. This work was funded by the Laboratory Directed Research and Development Program at LLNL under project tracking code 12-SI-005.

*murillo@lanl.gov

[1] R. Pakter and Y. Levin, Phys. Rev. Lett. **110**, 140601 (2013).
[2] K. P. Driver and B. Militzer, Phys. Rev. Lett. **108**, 115502 (2012).
[3] P. Hartmann, A. Douglass, J. C. Reyes, L. S. Matthews, T. W. Hyde, A. Kovacs, and Z. Donko, Phys. Rev. Lett. **105**, 115004 (2010).
[4] M. S. Murillo and M. W. C. Dharma-wardana, Phys. Rev. Lett. **100**, 205005 (2008).
[5] G. H. Miller, E. I. Moses, and C. R. Wuest, Nucl. Fusion **44**, S228 (2004).
[6] S. H. Glenzer and R. Redmer, Rev. Mod. Phys. **81**, 1625 (2009).
[7] D. O. Gericke, M. S. Murillo, and M. Schlanges, Phys. Rev. E **65**, 036418 (2002).
[8] G. Dimonte and J. Daligault, Phys. Rev. Lett. **101**, 135001 (2008).
[9] L. X. Benedict, M. P. Surh, J. I. Castor, S. A. Khairallah, H. D. Whitley, D. F. Richards, J. N. Glosli, M. S. Murillo, C. R. Scullard, P. E. Grabowski, D. Michta, and F. R. Graziani, Phys. Rev. E **86**, 046406 (2012).
[10] R. E. Rudd, W. H. Cabot, K. J. Caspersen, J. A. Greenough, D. F. Richards, F. H. Streitz, and P. L. Miller, Phys. Rev. E **85**, 031202 (2012).
[11] L. Burakovsky, C. Ticknor, J. D. Kress, L. A. Collins, and F. Lambert, Phys. Rev. E **87**, 023104 (2013).
[12] M. P. Desjarlais, J. D. Kress, and L. A. Collins, Phys. Rev. E **66**, 025401 (2002).
[13] F. Lambert, V. Recoules, A. Decoster, J. Clerouin, and M. Desjarlais, Phys. Plasmas **18**, 056306 (2011).
[14] M. Roth, T. E. Cowan, M. H. Key, S. P. Hatchett, C. Brown, W. Fountain, J. Johnson, D. M. Pennington, R. A. Snavely, S. C. Wilks, K. Yasuike, H. Ruhl, F. Pegoraro, S. V. Bulanov, E. M. Campbell, M. D. Perry, and H. Powell, Phys. Rev. Lett. **86**, 436 (2001).
[15] J. D. Lindl, P. Amendt, R. L. Berger, S. G. Glendinning, S. H. Glenzer, S. W. Haan, R. L. Kauffman, O. L. Landen, and L. J. Suter, Phys. Plasmas **11**, 339 (2004).
[16] D. A. Callahan-Miller and M. Tabak, Phys. Plasmas **7**, 2083 (2000).
[17] G. Zwicknagel, Nucl. Instrum. Methods Phys. Res., Sect. B **197**, 22 (2002).
[18] M. Ahsan Zeb, J. Kohanoff, D. Sánchez-Portal, A. Arnau, J. I. Juaristi, and Emilio Artacho, Phys. Rev. Lett. **108**, 225504 (2012).
[19] L. S. Brown, D. L. Preston, and R. L. Singleton, Jr., Phys. Rep. **410**, 237 (2005).
[20] Z.-H. Hu, Y.-H. Song, and Y.-N. Wang, Phys. Rev. E **82**, 026404 (2010).
[21] J. D. Huba, *NRL Plasma Formulary* (Naval Research Laboratory, Washington, DC, 2009).
[22] C.-K. Li and R. D. Petrasso, Phys. Rev. Lett. **70**, 3059 (1993).
[23] A. A. Solodov and R. Betti, Phys. Plasmas **15**, 042707 (2008).
[24] G. Zwicknagel and C. Deutsch, Phys. Rev. E **56**, 970 (1997).
[25] R. L. Liboff, *Kinetic Theory: Classical, Quantum, and Relativistic Descriptions, Graduate Texts in Contemp. Phys.* (Springer, New York, 2003).
[26] D. F. Richards, J. N. Glosli, B. Chan, M. R. Dorr, E. W. Draeger, J.-L. Fattebert, W. D. Krauss, T. Spelce, F. H. Streitz, M. P. Surh, and J. A. Gunnels, *Proceedings of the Conference on High Performance Computing Networking, Storage and Analysis, SC '09* (ACM, New York, 2009), p. 60.
[27] F. R. Graziani, V. S. Batista, L. X. Benedict, J. I. Castor, H. Chen, S. N. Chen, C. A. Fichtl, J. N. Glosli, P. E. Grabowski, A. T. Graf, S. P. Hau-Riege, A. U. Hazi, S. A. Khairallah, L. Krauss, A. Bruce Langdon, R. A. London, A. Markmann, M. S. Murillo, D. F. Richards, H. A. Scott, R. Shepherd, L. G. Stanton, F. H. Streitz, M. P. Surh, J. C. Weisheit, and H. D. Whitley, High Energy Density Phys. **8**, 105 (2012).
[28] G. Zwicknagel, C. Toepffer, and P.-G. Reinhard, Phys. Rep. **309**, 117 (1999).
[29] G. Zwicknagel, Ph.D. thesis, Friedrich-Alexander Universitat Erlangen-Nurnberg, 2000.
[30] T. Peter and J. Meyer-ter Vehn, Phys. Rev. A **43**, 1998 (1991).
[31] N. Bohr, Philos. Mag. **30**, 581 (1915).
[32] S. A. Khrapak, A. V. Ivlev, G. E. Morfill, S. K. Zhdanov, and H. M. Thomas, IEEE Trans. Plasma Sci. **32**, 555 (2004).
[33] S. Ichimaru, H. Iyetomi, and S. Tanaka, Phys. Rep. **149**, 91 (1987).
[34] S. D. Baalrud and J. Daligault, Phys. Rev. Lett. **110**, 235001 (2013).
[35] J. W. Dufty and M. Berkovsky, Nucl. Instrum. Methods Phys. Res., Sect. B **96**, 626 (1995).
[36] J. W. Dufty, B Talin, and A Calisti, Adv. Quantum Chem. **46**, 293 (2004).
[37] J. Hughto, A. S. Schneider, C. J. Horowitz, and D. K. Berry, Phys. Rev. E **82**, 066401 (2010).
[38] I. Binas and I. Mryglod, Condens. Matter Phys. **12**, 647 (2009).
[39] M. J. Nuevo, J. J. Morales, and D. M. Heyes, Phys. Rev. E **51**, 2026 (1995).
[40] H. A. Gould and H. E. DeWitt, Phys. Rev. **155**, 68 (1967).
[41] G. Zwicknagel and C. Deutsch, Phys. Rev. E **56**, 970 (1997).